crystals

MDPI

Article

The Effects of Chlorine Doping on the Mechanical Properties of Bi_2O_2Se

Buda Li [1], Hangbo Qi [2], Menglu Li [2], Xiaotao Zu [2], Liang Qiao [2,*] and Haiyan Xiao [1,*]

[1] Yangtze Delta Region Institute (Huzhou), University of Electronic Science and Technology of China, Huzhou 313001, China; libuda66@163.com
[2] School of Physics, University of Electronic Science and Technology of China, Chengdu 611731, China; qihangbo@u.nus.edu (H.Q.); mengluli0121@163.com (M.L.); xtzu@uestc.edu.cn (X.Z.)
* Correspondence: liang.qiao@uestc.edu.cn (L.Q.); hyxiao@uestc.edu.cn (H.X.)

Abstract: In this work, first-principle calculations based on density functional theory are employed to investigate how chlorine doping influences the elastic moduli, ductility, and lattice thermal conductivity of Bi_2O_2Se, aiming to explore an effective method to improve its mechanical properties for its applications under thermal stress. Our findings reveal that chlorine(Cl) doping significantly affects the electronic structure and mechanical properties of Bi_2O_2Se. The electrons are distributed on the Fermi level, and the Cl-doped Bi_2O_2Se exhibits metal-like properties. In addition, Cl doping enhances the ductility and toughness of Bi_2O_2Se and reduces its lattice thermal conductivity. These results suggest that Cl doping is an effective approach for tuning the mechanical properties of Bi_2O_2Se.

Keywords: density functional theory; Bi_2O_2Se; chlorine doping; electronic structure; mechanical properties

Citation: Li, B.; Qi, H.; Li, M.; Zu, X.; Qiao, L.; Xiao, H. The Effects of Chlorine Doping on the Mechanical Properties of Bi_2O_2Se. *Crystals* **2023**, *13*, 1492. https://doi.org/10.3390/cryst13101492

Academic Editors: Danny A Rehn, Ann E. Mattsson, Roxanne Tutchton, Jian-Xin Zhu and Christopher Lane

Received: 22 September 2023
Revised: 8 October 2023
Accepted: 10 October 2023
Published: 13 October 2023

1. Introduction

Presently, in the face of the escalating global energy crisis and increasing environmental pollution, it is imperative to develop green and sustainable energy resources [1,2]. Thermoelectric power generation (TEG) has become one of the hot research topics due to its advantages of being green and efficient [3]. The assembly, manufacturing process, and reliable operation of TEG devices necessitate thermoelectric materials with excellent mechanical performance. Inferior mechanical properties can lead to crack formation and subsequent performance degradation under thermal stress, especially considering the operational conditions involving cyclic temperature gradients [4,5]. Therefore, it is essential for materials to possess favorable mechanical properties in order to meet the requirements of practical applications.

In recent years, Bismuth oxyselenide (Bi_2O_2Se), in which weak electrostatic interactions exist between adjacent layers, has attracted widespread attention and become an emerging structural material with great development potential in high-performance electronic, optoelectronic, and flexible devices due to its high electron mobility and excellent air stability [6,7]. So far, experimental and theoretical investigations on the mechanical properties of Bi_2O_2Se are still in their infancy stage. Theoretically, Liu et al. [8] investigated the electronic structure, bulk modulus, shear modulus, and thermal conductivity of Bi_2O_2Se using density functional theory (DFT), and revealed its high anisotropy and potential as a mechanical material. Pang et al. [9] studied the mechanical response of Bi_2O_2Se under uniaxial and biaxial tension using first-principles calculations. They found that the band gap of Bi_2O_2Se decreases with increasing tensile strain, and a phase transition from semiconductor to metal occurs eventually, due to the evolution of electron localization function. Wang et al. [10] studied the mechanical properties of Bi_2O_2Se under a pressure of 50 GPa using first-principles calculations and found that the Bi_2O_2Se exhibits mechanical stability at least below 50 GPa. Furthermore, the Bi_2O_2Se exhibits anisotropic and malleable

properties within the pressure range, with the anisotropy becoming increasingly significant as the pressure increases. Zhang et al. [11] studied the elastic properties of $Bi_2O_2Se_{1-x}Te_x$ by the first-principles calculations and proposed that substituting Se for Te in Bi_2O_2Se can optimize its mechanical properties. Despite these efforts, further improvements on the mechanical properties of Bi_2O_2Se are necessary in order to meet the requirements of thermoelectric generator device assembly and manufacturing processes, as well as to ensure reliable operation.

Experimentally, the halogen element Cl has been widely employed to enhance the mechanical properties of materials. Piriz et al. [12] investigated the mechanical properties of Cl-doped edge zigzag graphene nanoribbons (ZGNRs) and found that Cl-doped ZGNRs exhibit better mechanical properties as compared to pure graphene. Zhang et al. [13] prepared Cl-doped carbon nanotube sheets via floating catalyst chemical vapor deposition and studied the effects of Cl doping on the mechanical properties of carbon nanotube sheets. They found that the doped sandwich composite film displays excellent mechanical properties, with a tensile strength of 90 MPa. Theoretically, Park et al. [14] investigated the effect of Cl doping on the mechanical properties of amorphous carbon films using DFT and revealed that the introduction of Cl atoms into amorphous carbon films could significantly reduce the bulk modulus, thereby softening the films. These experimental and computational studies demonstrate that Cl doping is an effective approach for improving the mechanical properties of materials.

However, the research on the mechanical properties of Cl-doped Bi_2O_2Se has not been reported thus far. Therefore, in this work, we employ first-principles methods to investigate the effects of Cl doping on the geometrical, electronic, and mechanical properties of Bi_2O_2Se. The geometrical structure, density of state distributions, bulk modulus B, Young's modulus E, shear modulus G, Debye temperature θ_D, and lattice thermal conductivity κ_l are all determined for Bi_2O_2Se before and after Cl doping. It is shown that Cl doping results in redistribution of electrons in Bi_2O_2Se, and the Cl-doped Bi_2O_2Se exhibits metallic properties. In addition, Cl doping affects the mechanical strength, toughness, ductility, and lattice thermal conductivity of Bi_2O_2Se considerably. As compared with the pristine Bi_2O_2Se, the Cl-doped system exhibits better ductility, better toughness, and reduced lattice thermal conductivity, which is beneficial to restrain heat transfer and reduce the heat loss of energy. This study, thus, provides a new method to tune the physical properties of Bi_2O_2Se and has important implications for promoting related investigations.

2. Computational Details

Our calculations are implemented in the Ab initio Simulation Package (VASP) code (Vienna, Austria) within the framework of DFT [15]. The interaction between electrons and ions is described by the projector augmented-wave (PAW) pseudopotential approximation [16]. In addition, the Perdew–Burke–Ernzerhof (PBE) functional within the generalized gradient approximation (GGA) [17] and the Heyd–Scuseria–Ernzerhof (HSE06) hybrid functional [18] are used to deal with the exchange-correlation potential between electrons. The Monkhorst-package scheme [19] with a $6 \times 6 \times 6$ k-point sampling for the Brillouin-zone is used to perform all the calculations. Besides, the cut-off energy for the plane wave basis sets is 500 eV. In this work, the considered systems are Bi_2O_2Se and $Bi_2O_2Se_{0.875}Cl_{0.125}$. The elastic constants of the material are calculated by using the stress-strain method, in which six finite distortions of the lattice are performed, and the relationship between the stress component σ_i (i = 1–6) and the applied strain ε_j (j = 1–6) at a small deformation is described as $\sigma_i = \sum_{j=1}^{6} C_{ij}\varepsilon_j$ [20]. In the calculation, the energy and force convergence criteria are set to be 1×10^{-5} eV/atom and 1×10^{-2} eV/Å, respectively. The specific flowchart of the calculation process is shown in Figure 1.

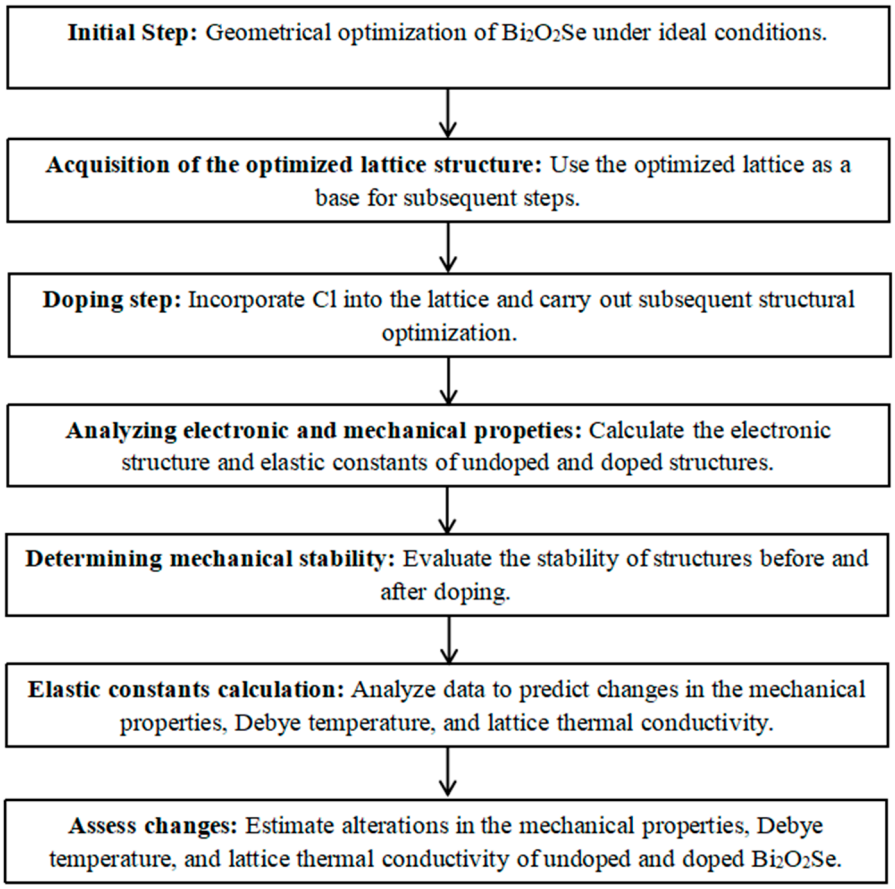

Figure 1. Flowchart of the calculation process for undoped and doped Bi_2O_2Se.

3. Results and Discussions

3.1. Structural Properties of Bi_2O_2Se and $Bi_2O_2Se_{0.875}Cl_{0.125}$

The bulk phase of Bi_2O_2Se exhibits a tetragonal I4/mmm structure (No. 139) with a unit cell containing 10 atoms. Within Bi_2O_2Se, the curved $[Bi_2O_2]^{2+}$ layers and $[Se]^{2-}$ layers stack alternately along the c-axis through weak electrostatic interactions [21]. Figure 2 presents the optimized geometrical structure of Bi_2O_2Se and $Bi_2O_2Se_{0.875}Cl_{0.125}$, both containing 40 atoms. The lattice constants, volumes, and bond lengths of Bi_2O_2Se and $Bi_2O_2Se_{0.875}Cl_{0.125}$ are presented in Table 1. For undoped Bi_2O_2Se, the calculated lattice constants are $a_0 = b_0 = 3.917$ Å and $c_0 = 12.357$ Å, which show good agreements with other computational results of $a_0 = b_0 = 3.90$ Å and $c_0 = 12.39$ Å [22], as well as experimental data of $a_0 = b_0 = 3.88$ Å and $c_0 = 12.16$ Å [23]. Additionally, the <Bi-O> and <Bi-Se> bond lengths of Bi_2O_2Se are determined to be 2.337 Å and 3.311 Å, respectively. These values are comparable with the previously calculated results of 2.312 Å and 3.272 Å reported by Wu et al. [24]. As compared with Bi_2O_2Se, the calculated lattice constants a_0 and b_0 (3.946 Å) of $Bi_2O_2Se_{0.875}Cl_{0.125}$ are increased by 0.74%, while the c_0 (12.287 Å) is decreased by 0.57%, resulting in a 0.91% volume expansion. Meanwhile, the calculated <Bi-O> bond length (2.339 Å) of $Bi_2O_2Se_{0.875}Cl_{0.125}$ is increased by 0.09% and <Bi-Se> bond length (3.336 Å) is increased by 0.76%. This is mainly because the following reactions occur after Cl doping [25]:

$$Cl^- \overset{Se^{2-}}{\rightarrow} Cl_{Se}^{\cdot} + e', \quad (1)$$

where extra electrons are produced, resulting in increased repulsive interaction between electrons and an expansion of volume.

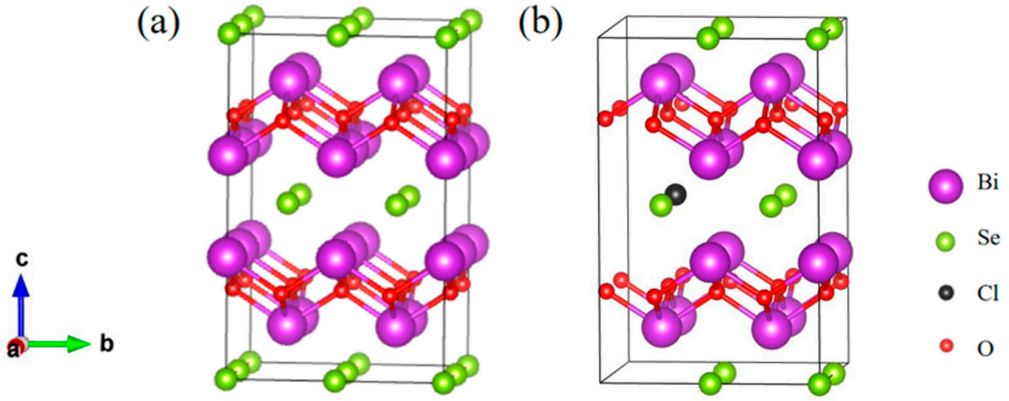

Figure 2. The optimized geometrical structures of (**a**) Bi_2O_2Se and (**b**) $Bi_2O_2Se_{0.875}Cl_{0.125}$. The purple, green, black and red spheres denote Bi, Se, Cl and O atoms, respectively.

Table 1. Comparison of lattice constants a_0 (Å) and c_0 (Å), volume (Å^3), and bond length (Å) of Bi_2O_2Se and $Bi_2O_2Se_{0.875}Cl_{0.125}$ with experimental and other theoretical results.

		a_0	c_0	Volume	<Bi-O>	<Bi-Se>
Bi_2O_2Se	Our cal.	3.917	12.357	189.592	2.337	3.311
	Exp. [23]	3.88	12.16	183.06	---	---
	Other cal. [22]	3.90	12.39	188.45	---	---
$Bi_2O_2Se_{0.875}Cl_{0.125}$	Our cal.	3.946	12.287	191.320	2.339	3.336

3.2. The Influence of Cl Doping on the Electronic Structure of Bi_2O_2Se

We further explore the influence of Cl doping on the electronic structure of Bi_2O_2Se by investigating the density of state (DOS) distributions of Bi_2O_2Se and $Bi_2O_2Se_{0.875}Cl_{0.125}$. The total and projected DOS distributions around the Fermi level of Bi_2O_2Se and $Bi_2O_2Se_{0.875}Cl_{0.125}$, obtained by the standard DFT method, are plotted in Figure 3a,b, respectively. For Bi_2O_2Se, the valence bands ranging from 4 to 5.53 eV are predominantly dominated by Se 4*p* orbitals hybridized with O 2*p* and Bi 6*s* orbitals. The conduction bands ranging from 6.02 to 8 eV are mainly characterized by Bi 6*p* orbitals and O 2*p* orbitals. The obtained band gap between the valence band maxima (contributed by Bi 6*s*) and the conduction band minima (contributed by Bi 6*p*) of 0.49 eV for Bi_2O_2Se is consistent with previous theoretical values (0.41 eV [26], 0.43 eV [27], and 0.472 eV [28]). In addition, the strong hybridization between these orbitals will lead to higher stability in Bi_2O_2Se [29]. The DOS distributions of $Bi_2O_2Se_{0.875}Cl_{0.125}$ shown in Figure 3b indicate that the Fermi levels cross the valence bands and conduction bands, and many electrons are observed at the Fermi level. These features imply metallic properties for $Bi_2O_2Se_{0.875}Cl_{0.125}$, which differ from the results reported by Tan et al. [25], primarily because our doping concentration of 2.5% is higher than the dissolution limit of 1.5% in the literature.

Due to the underestimation of band gap values in standard DFT calculations, we further use the hybrid DFT method to calculate the total and projected DOS distributions around the Fermi level of Bi_2O_2Se and $Bi_2O_2Se_{0.875}Cl_{0.125}$, and the calculated results are displayed in Figure 3c,d. For Bi_2O_2Se, the calculated band gap between the valence band maxima (contributed by Bi 6*s*) and the conduction band minima (contributed by Bi 6*p*) is 1.05 eV, which is consistent with the previous computational values of 0.9 eV [30], 0.99 eV [8] and 1.01 eV [31]. Nonetheless, our hybrid DFT value is larger than the corresponding experimental value of 0.85 eV [24]. We note that due to the inclusion of a mixture of Hartree-Fock (HF) and DFT exchange terms, hybrid DFT calculations may overestimate or underestimate material band gaps [32,33], leading to higher or lower calculated values relative to their experimental counterparts [34]. The hybrid DFT, thus, represents a practical, although not perfect, solution to reproduce experimental band gaps. For $Bi_2O_2Se_{0.875}Cl_{0.125}$, it can be seen that the electron distribution obtained by the hybrid DFT method is more

delocalized, as compared with the standard DFT results, and a certain number of electrons are still distributed at the Fermi level, i.e., the doped Bi_2O_2Se shows metal-like properties.

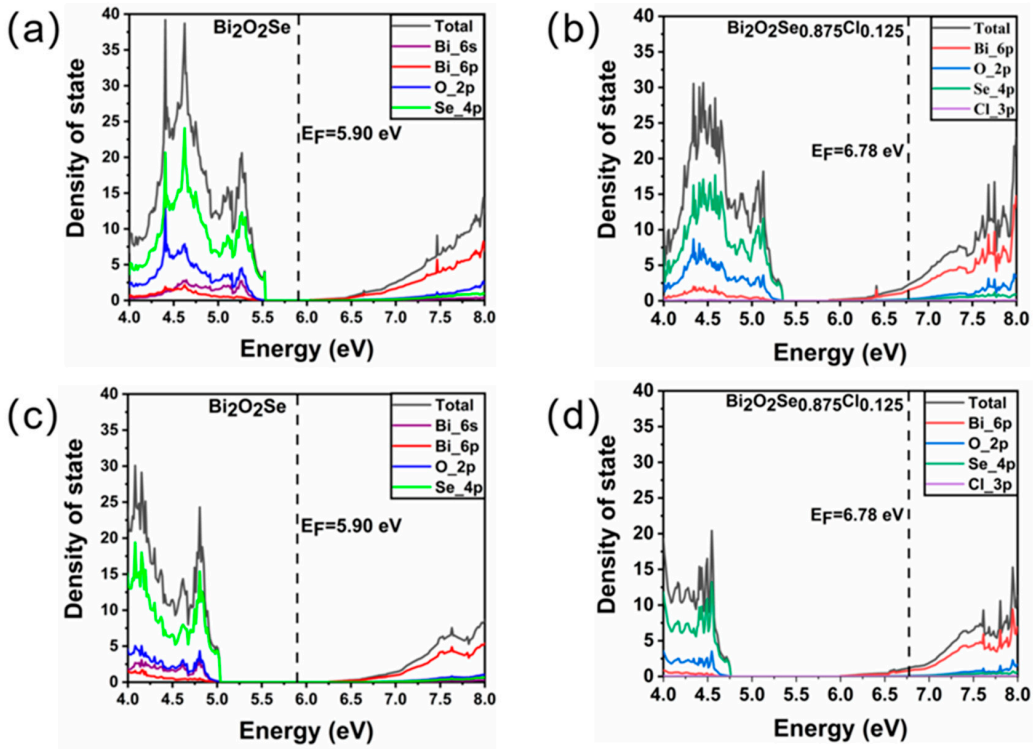

Figure 3. The total and projected density of state distribution for Bi_2O_2Se and $Bi_2O_2Se_{0.875}Cl_{0.125}$ obtained by (**a**,**b**) standard DFT method and (**c**,**d**) hybrid DFT method. The E_F denotes the Fermi energy.

3.3. Mechanical Properties of Bi_2O_2Se and $Bi_2O_2Se_{0.875}Cl_{0.125}$

3.3.1. Elastic Constants of Bi_2O_2Se and $Bi_2O_2Se_{0.875}Cl_{0.125}$

The elastic constants (C_{ij}) of Bi_2O_2Se and $Bi_2O_2Se_{0.875}Cl_{0.125}$ are first calculated based on the optimized geometrical structures. The Bi_2O_2Se possesses a tetragonal crystal structure, resulting in six independent elastic constants, namely C_{11}, C_{12}, C_{13}, C_{33}, C_{44} and C_{66} [8]. The calculated elastic constants are shown in Table 2 and compared with other literature values [8]. The calculated elastic constants for Bi_2O_2Se, i.e., C_{11} = 159.39 GPa, C_{12} = 73.55 GPa, C_{13} = 44.24 GPa, C_{33} = 121.28 GPa, C_{44} = 13.41 GPa, and C_{66} = 57.71 GPa, are in good agreement with previous computational results of C_{11} = 155.48 GPa, C_{12} = 71.56 GPa, C_{13} = 43.47 GPa, C_{33} = 119.01 GPa, C_{44} = 11.23 GPa, and C_{66} = 56.41 GPa [8]. Moreover, the calculated elastic constant C_{11} (159.39 GPa) is found to be larger than C_{33} (121.28 GPa), indicating that the Bi_2O_2Se exhibits higher resistance to deformation along the <100> direction as compared to the <001> direction. Moreover, the calculated value of C_{13} (44.24 GPa) is smaller than that of C_{12} (73.55 GPa), which indicates that the Bi_2O_2Se exhibits more significant contraction along the <001> direction as compared to the <010> direction when applying the same normal stress along the <100> direction. Furthermore, our results show that C_{66} (57.71 GPa) is larger than C_{44} (13.41 GPa), indicating that shear deformation along the (001) plane is more difficult to occur as compared to shear deformation along the (100) plane for Bi_2O_2Se [35,36].

As compared with the values of Bi_2O_2Se, the calculated elastic constants C_{11} = 143.17 GPa, C_{12} = 63.39 GPa, C_{33} = 106.87 GPa, C_{44} = 11.96 Gpa, and C_{66} = 53.74 GPa for $Bi_2O_2Se_{0.875}Cl_{0.125}$ are reduced by 10.18%, 13.81%, 11.88%, 10.81%, and 6.88%, respectively, while the calculated value of C_{13} (46.38 GPa) is increased by 4.84%. These results suggest that Cl doping has significant effects on the mechanical properties of Bi_2O_2Se. Furthermore, the mechanical stability of Bi_2O_2Se and $Bi_2O_2Se_{0.875}Cl_{0.125}$ are determined by employing the following equation:

$$C_{11} > 0,\ C_{33} > 0,\ C_{44} > 0,\ C_{66} > 0, (C_{11} - C_{12}) > 0, \quad (2)$$

$$(C_{11} + C_{33} - 2C_{13}) > 0,\ [2(C_{11} + C_{12}) + C_{33} + 4C_{13}] > 0. \quad (3)$$

Our calculations demonstrate that both Bi_2O_2Se and $Bi_2O_2Se_{0.875}Cl_{0.125}$ satisfy the above mechanical stability criteria.

Table 2. The calculated elastic constants (C_{11}, C_{12}, C_{13}, C_{33}, C_{44} and C_{66} in GPa) for Bi_2O_2Se and $Bi_2O_2Se_{0.875}Cl_{0.125}$.

Compounds		C_{11}	C_{12}	C_{13}	C_{33}	C_{44}	C_{66}
Bi_2O_2Se	Our Cal.	159.39	73.55	44.24	121.28	13.41	57.71
	Other Cal. [8]	155.48	71.56	43.47	119.01	11.23	56.41
$Bi_2O_2Se_{0.875}Cl_{0.125}$	Our Cal.	143.17	63.39	46.38	106.87	11.96	53.74

3.3.2. Elastic Moduli of Bi_2O_2Se and $Bi_2O_2Se_{0.875}Cl_{0.125}$

The bulk modulus (B), shear modulus (G) and Young's modulus (E) of Bi_2O_2Se and $Bi_2O_2Se_{0.875}Cl_{0.125}$ can be calculated by using the Voigt–Reuss–Hill (VRH) approximation method [37]. In VRH approximation, the Voigt [38] and Reuss [39] approximations correspond to the upper and lower limits of the modulus, respectively. According to the Voigt approximation, the bulk modulus (B_V) and shear modulus (G_V) can be calculated by the following equations:

$$B_V = \frac{1}{9[2C_{11} + 2C_{12} + C_{33} + 4C_{13}]}, \quad (4)$$

$$G_V = \frac{1}{15}\left[(C_{11} + C_{22} + C_{13}) - (C_{12} + C_{23} + C_{31}) + 3(C_{44} + C_{55} + C_{66})\right]. \quad (5)$$

The bulk modulus (B_R) and shear modulus (G_R) can also be calculated by the Reuss approximation:

$$B_R = \frac{(C_{11} + C_{12})C_{33} - 2C_{13}^2}{C_{11} + C_{12} + 2C_{33} - 4C_{13}}, \quad (6)$$

$$G_R = \frac{15}{18B_V/[(C_{11} + C_{12})C_{33} - 2C_{13}^2] + 6/(C_{11} - C_{12}) + 6/C_{44} + 3/C_{66}} \quad (7)$$

Then, the elastic modulus is the arithmetic average of the Voigt and Reuss approximations, which can be expressed as:

$$B = \frac{B_V + B_R}{2}, \quad (8)$$

$$G = \frac{G_V + G_R}{2} \quad (9)$$

Further, the Young's modulus (E) can be given by:

$$E = \frac{9BG}{3B + G}. \quad (10)$$

The calculated results are shown in Table 3, along with other results [8,40,41] for comparison. For Bi_2O_2Se, the calculated elastic moduli are B = 83.21 GPa, G = 29.59 Gpa, and E = 79.36 GPa, which agree well with the calculated results of B = 81.42 GPa, G = 27.38 GPa, and E = 73.56 GPa [8]. Besides, the calculated results of B = 83.21 GPa and E = 79.36 GPa are comparable to the experimental values of B = 71.5 GPa reported by Mahan et al. [41] and E = 66 GPa reported by Sagar et al. [40].

Table 3. The calculated bulk modulus B (GPa), shear modulus G (GPa) and Young's modulus E (GPa) for Bi_2O_2Se and $Bi_2O_2Se_{0.875}Cl_{0.125}$.

Compounds		B	G	E
Bi_2O_2Se	Our Cal.	83.21	29.59	79.36
	Other Cal. [8]	81.42	27.38	73.56
	Other Cal. [10]	---	---	---
	Exp. [40]	---	---	66
	Exp. [41]	71.5	---	---
$Bi_2O_2Se_{0.875}Cl_{0.125}$	Our Cal.	77.05	26.20	70.59

The B of $Bi_2O_2Se_{0.875}Cl_{0.125}$ is calculated to be 77.05 GPa, which is 7.40% lower than that of pure Bi_2O_2Se, indicating that the introduction of Cl dopant reduces the resistance of Bi_2O_2Se towards uniform compression. Moreover, Cl doping reduces the G of Bi_2O_2Se from 29.59 GPa to 26.20 GPa, indicating that the chemical bonds in $Bi_2O_2Se_{0.875}Cl_{0.125}$ are less strong and directional than those in Bi_2O_2Se, rendering it more susceptible to plastic deformation [42]. Furthermore, as compared with the calculated E of 79.36 GPa for Bi_2O_2Se, the calculated E = 70.59 GPa for $Bi_2O_2Se_{0.875}Cl_{0.125}$ is 11.05% smaller, i.e., the incorporation of Cl dopant in Bi_2O_2Se results in reduced tolerance to elastic deformation, thereby facilitating crack prevention under extreme temperature gradients [43]. In the literature, Zhang et al. [11] have reported that Te doping can reduce the elastic moduli of Bi_2O_2Se, which is similar to the phenomenon of Cl doping. In addition, the smaller B or E, the better the elastic compliance of materials. The presented results suggest that Cl doping enhances the elastic compliance of Bi_2O_2Se.

3.3.3. Ductility and Elastic Anisotropy of Bi_2O_2Se and $Bi_2O_2Se_{0.875}Cl_{0.125}$

Ductility is an important index to measure the mechanical properties of a material. It represents the ability of a material to exhibit significant plastic deformation without breaking under mechanical stress [44]. Based on the calculated elastic moduli, the B/G values and brittle-ductile behavior of Bi_2O_2Se and $Bi_2O_2Se_{0.875}Cl_{0.125}$ are further explored. The critical value for the brittle-ductile transition of the material is 1.75 [45,46]. When the B/G ratio is less than 1.75, the material exhibits brittleness; otherwise, it demonstrates ductility. The calculated B/G ratio for Bi_2O_2Se is 2.81, which is in close agreement with the value of 2.97 reported by MacIsaac et al. [47]. This result indicates that Bi_2O_2Se is a ductile material. For $Bi_2O_2Se_{0.875}Cl_{0.125}$, the calculated B/G value is 2.94, which is 4.63% higher than that of Bi_2O_2Se, suggesting that Cl doping enhances the ductility of Bi_2O_2Se, possibly due to the presence of metallic bonding in $Bi_2O_2Se_{0.875}Cl_{0.125}$.

Elastic anisotropy is another important mechanical property of materials, which is related to the appearance of microcracks [48,49]. The universal anisotropic index (A_U) of Bi_2O_2Se and $Bi_2O_2Se_{0.875}Cl_{0.125}$ is calculated using the following formula [8]:

$$A_U = \frac{5G_V}{G_R} + \frac{B_V}{B_R} - 6. \quad (11)$$

When the value of A_U is not equal to 0, the material exhibits elastic anisotropy. For Bi_2O_2Se, the calculated A_U value is 2.51, which indicates that Bi_2O_2Se is mechanically anisotropic. This finding is consistent with the conclusions drawn by Liu et al. [8]. Moreover, for $Bi_2O_2Se_{0.875}Cl_{0.125}$, the calculated A_U value is 2.47, which is close to the A_U value (2.51) of Bi_2O_2Se, indicating that Cl doping has slight impacts on the mechanical anisotropy of Bi_2O_2Se. The ELATE tool [50] can be utilized to generate directional plots of Young's modulus for Bi_2O_2Se and $Bi_2O_2Se_{0.875}Cl_{0.125}$. A more isotropic modulus will resemble a sphere in shape. As illustrated in Figure 4, the plot of Bi_2O_2Se and $Bi_2O_2Se_{0.875}Cl_{0.125}$ deviates from sphere shape, indicating that the Young's modulus of Bi_2O_2Se and $Bi_2O_2Se_{0.875}Cl_{0.125}$ is anisotropic.

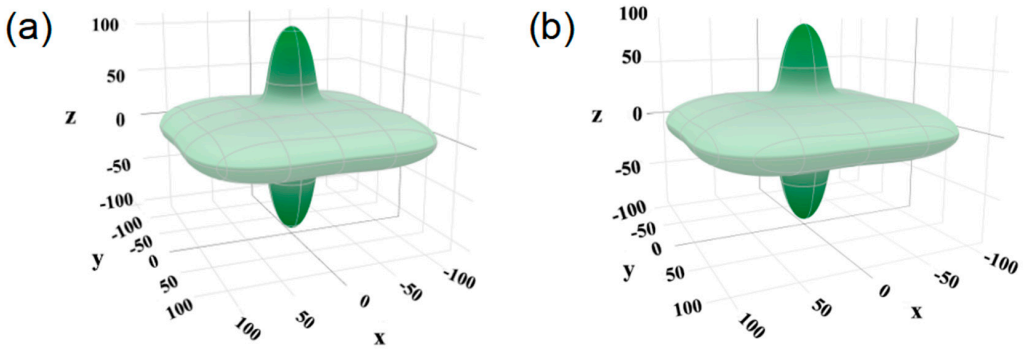

Figure 4. The directional dependence of Young's modulus E for (**a**) Bi_2O_2Se and (**b**) $Bi_2O_2Se_{0.875}Cl_{0.125}$. The unit is GPa, and each axis is the component of Young's modulus along that axis.

3.3.4. Debye Temperature of Bi_2O_2Se and $Bi_2O_2Se_{0.875}Cl_{0.125}$

The Debye temperature θ is the characterization of binding force between atoms, and the specific formula is [51]:

$$\theta = \frac{h}{k_B}\left(\frac{3n}{4\pi\Omega}\right)^{1/3} v_a\,, \tag{12}$$

where h and k_B are the Planck constant and Boltzmann constant, respectively. The Ω represents cell volume, n represents number of atoms in the cell, and v_a is the average sound wave velocity. The v_a can be calculated by [52,53]:

$$v_a = \left[\frac{1}{3}\left(\frac{1}{v_L^3} + \frac{2}{v_T^3}\right)\right]^{-1/3}. \tag{13}$$

Here, the v_L and v_T are the longitudinal and transverse sound wave velocity, respectively, which can be calculated by [54]:

$$v_L = \sqrt{\frac{E(1-v)}{\rho(1+v)(1-2v)}} = \sqrt{\frac{B+4/3G}{\rho}}, \tag{14}$$

$$v_T = \sqrt{\frac{E}{2\rho(1+v)}} = \sqrt{\frac{G}{\rho}}. \tag{15}$$

The calculated results are shown in Table 4, along with other results [8,10] for comparison. The calculated average sound velocity for Bi_2O_2Se is 2007 m/s, which is comparable to the value of 1939 m/s calculated by Liu et al. [8], but different from the calculated results of 1600 m/s reported by Wang et al. [10]. This is mainly because in the calculations of Wang et al. they used the CASTEP code with ultrasoft pseudopotentials, whereas we employ the VASP code with PAW pseudopotentials. Therefore, their calculated Debye temperature of 224.1 K is different from our calculated value of 181.0 K [10]. For $Bi_2O_2Se_{0.875}Cl_{0.125}$, our calculated Debye temperature θ (212.5 K) is 11.6 K smaller than that of pure Bi_2O_2Se (224.1 K), indicating that the atomic binding force in Bi_2O_2Se is reduced by Cl doping, due to the weakened covalency of chemical bonds [55], which will be beneficial to improve the toughness and processing performance of Bi_2O_2Se.

Table 4. The calculated transverse wave velocity v_T (m/s), longitudinal wave velocity v_L (m/s), average wave velocity v_a (m/s), and Debye temperature θ (K) for Bi_2O_2Se and $Bi_2O_2Se_{0.875}Cl_{0.125}$.

Compounds		v_L	v_T	v_a	θ
Bi_2O_2Se	Our Cal.	3638	1787	2007	224.1
	Other Cal. [8]	3584	1727	1939	--
	Other Cal. [10]	1440	2630	1600	181.0
$Bi_2O_2Se_{0.875}Cl_{0.125}$	Our Cal.	3513	1699	1909	212.5

3.3.5. Lattice Thermal Conductivity κ_l of Bi_2O_2Se and $Bi_2O_2Se_{0.875}Cl_{0.125}$

The Slack equation [56] can be used to calculate the lattice thermal conductivity κ_l:

$$\kappa_\iota = A \cdot \frac{\overline{M}\,\Theta^3 \delta}{\gamma^2 T n^{\frac{2}{3}}}. \quad (16)$$

Here, A is a constant, and the calculation formula is given by:

$$A = 2.43 \times \frac{10^{-6}}{1 - \frac{0.514}{\gamma} + \frac{0.228}{\gamma^2}}. \quad (17)$$

In this equation, $\overline{M}$ represents the average atomic mass, δ^3 is the volume of each atom, γ is the Grüneisen parameter, Θ is the Debye temperature, and T is the absolute temperature. The Slack model has been demonstrated to provide lattice thermal conductivity results that agree well with experimental measurements, and has been extensively used in the calculation of lattice thermal conductivity of materials [30,57]. Figure 5 shows the temperature-dependent results of κ_l. It is observed that the lattice thermal conductivity of both Bi_2O_2Se and $Bi_2O_2Se_{0.875}Cl_{0.125}$ decreases with increasing temperature. For Bi_2O_2Se, the calculated κ_l at 300 K is 1.68 W/mK, which agrees well with the experimental data of κ_l = 1.8 W/mK and other calculated results of κ_l = 1.2 W/mK [31]. Furthermore, Cl doping reduces the lattice thermal conductivity of Bi_2O_2Se. For example, the calculated lattice thermal conductivity of $Bi_2O_2Se_{0.875}Cl_{0.125}$ at 300 K is 1.29 W/mK, which is 23.21% smaller than that of Bi_2O_2Se (1.68 W/mK). This is mainly due to the low elastic constants of $Bi_2O_2Se_{0.875}Cl_{0.125}$. The reduced lattice thermal conductivity will be beneficial for suppressing heat transfer and minimizing thermal energy loss. $Bi_2O_2Se_{0.875}Cl_{0.125}$ exhibits metallic character and electrons should also contribute to the thermal transport of Bi_2O_2Se. Considering that the Bi_2O_2Se is a semiconductor and its thermal conductivity is mainly contributed by phonons, and this work mainly focuses on the effect of Cl doping on the thermal transport properties of Bi_2O_2Se, the electronic thermal conductivity of Cl-doped Bi_2O_2Se, thus, is not considered in this work.

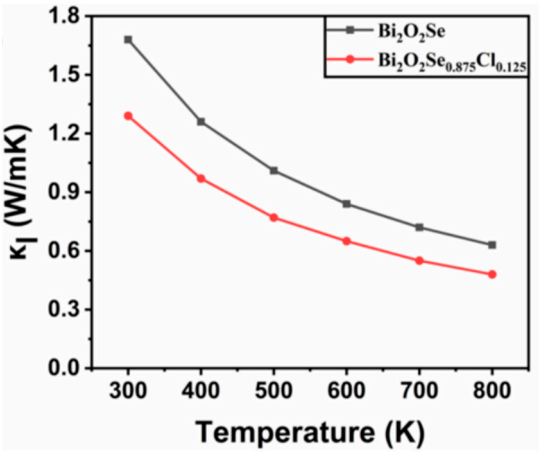

Figure 5. The calculated lattice thermal conductivity κ_l of Bi_2O_2Se and $Bi_2O_2Se_{0.875}Cl_{0.125}$ as a function of temperature.

4. Conclusions

In this work, the effect of Cl doping on the structural, electronic, and mechanical properties of Bi_2O_2Se is investigated by using the first-principles calculations based on the DFT method. The main results are summarized as follows:

1. The Cl doping results in an increase of 0.74% in the lattice constant a_0 (3.946 Å) of Bi_2O_2Se, while c_0 (12.287 Å) is decreased by 0.57% and the volume is expanded by

0.91%. At the same time, the calculated <Bi-O> bond lengths (2.339 Å) is increased by 0.09%, and the <Bi-Se> bond length (3.336 Å) is increased by 0.76%.

2. The Cl doping has significant influences on the electronic structure of Bi_2O_2Se. Different from the semiconductor character of the pristine Bi_2O_2Se, the $Bi_2O_2Se_{0.875}Cl_{0.125}$ exhibits metallic properties, since a certain number of electrons are distributed at the Fermi level.
3. As compared with the elastic constants of Bi_2O_2Se, the calculated elastic constants C_{11} = 143.17 GPa, C_{12} = 63.39 GPa, C_{33} = 106.87 GPa, C_{44} = 11.96 GPa and C_{66} = 53.74 GPa for $Bi_2O_2Se_{0.875}Cl_{0.125}$ are reduced by 10.18%, 13.81%, 11.88%, 10.81%, and 6.88%, respectively, while the calculated value of C_{13} (46.38 GPa) is increased by 4.84%. These results suggest that Cl doping has remarkable effects on the mechanical properties of Bi_2O_2Se. Both the doped and undoped Bi_2O_2Se satisfy the criteria of mechanical stability and exhibit elastic anisotropy.
4. The Cl doping leads to a reduction of 7.40%, 11.46%, and 11.05% in the bulk modulus, shear modulus, and Young's modulus of Bi_2O_2Se, respectively, suggesting that Cl doping leads to a more plastic deformation of Bi_2O_2Se, which could help to prevent cracking under extreme temperature gradients.
5. The calculated B/G value of $Bi_2O_2Se_{0.875}Cl_{0.125}$ is 2.94, which is 4.63% higher than that of pure Bi_2O_2Se, indicating that Cl doping enhances the ductility of Bi_2O_2Se.
6. The calculated Debye temperature θ of $Bi_2O_2Se_{0.875}Cl_{0.125}$ is 212.5 K, which is 11.6 K lower than that of pure Bi_2O_2Se (224.1 K). This lower Debye temperature helps to improve the toughness and processability of Bi_2O_2Se.
7. The lattice thermal conductivity of both Bi_2O_2Se and $Bi_2O_2Se_{0.875}Cl_{0.125}$ decreases with increasing temperature. Cl doping reduces the lattice thermal conductivity of Bi_2O_2Se considerably. For example, the lattice thermal conductivity of $Bi_2O_2Se_{0.875}Cl_{0.125}$ at 300 K is 1.29 W/mK, which is 23.21% lower than that of pure Bi_2O_2Se (1.68 W/mK). The lower lattice thermal conductivity is beneficial in inhibiting heat transfer and minimizing thermal energy loss.

Generally, Cl doping leads to an improvement in the mechanical properties and a decrease in the lattice thermal conductivity of Bi_2O_2Se. Therefore, it is suggested that the Cl-doped Bi_2O_2Se can be used to develop TEG materials with good thermoelectric and mechanical properties.

Author Contributions: Conceptualization, B.L. and H.X.; methodology, H.X., H.Q., M.L. and X.Z.; software, H.X.; validation, B.L., H.Q. and M.L.; formal analysis, B.L. and H.Q.; investigation, B.L.; resources, X.Z., H.X. and L.Q.; data curation, B.L.; writing—original draft preparation, B.L.; writing—review and editing, H.X. and L.Q.; visualization, B.L.; supervision, H.Q., M.L. and H.X.; project administration, B.L.; funding acquisition, H.X. and L.Q. All authors have read and agreed to the published version of the manuscript.

Funding: This research received no external funding.

Data Availability Statement: The datasets generated during and/or analyzed during the current study are available from the corresponding author on reasonable request.

Acknowledgments: H. Y. Xiao was supported by the Joint Funds of the National Natural Science Foundation of China (Grant No. U1930120). L.Q. acknowledges the support of the National Natural Science Foundation of China (Grant No. 52072059). All the calculations in this paper have been carried out on Hefei advanced computing center.

Conflicts of Interest: The authors declare no conflict of interest.

References

1. Wang, N.; Li, M.; Xiao, H.; Gao, Z.; Liu, Z.; Zu, X.; Li, S.; Qiao, L. Band degeneracy enhanced thermoelectric performance in layered oxyselenides by first-principles calculations. *npj Computat. Mater.* **2021**, *7*, 18. [CrossRef]
2. Wang, N.; Li, M.; Xiao, H.; Zu, X.; Qiao, L. Layered LaCuOSe: A Promising Anisotropic Thermoelectric Material. *Phys. Rev. Appl.* **2020**, *13*, 024038. [CrossRef]

3. Liu, W.; Jie, Q.; Kim, H.S.; Ren, Z. Current progress and future challenges in thermoelectric power generation: From materials to devices. *Acta Mater.* **2015**, *87*, 357–376. [CrossRef]
4. Yang, J.; Stabler, F.R. Automotive Applications of Thermoelectric Materials. *J. Electron. Mater.* **2009**, *38*, 1245–1251. [CrossRef]
5. Wang, N.; Shen, C.; Sun, Z.; Xiao, H.; Zhang, H.; Yin, Z.; Qiao, L. High-Temperature Thermoelectric Monolayer Bi_2TeSe_2 with High Power Factor and Ultralow Thermal Conductivity. *ACS Appl. Energy Mater.* **2022**, *5*, 2564–2572. [CrossRef]
6. Ren, D.S.; Feng, X.N.; Liu, L.S.; Hsu, H.J.; Lu, L.G.; Wang, L.; He, X.M.; Ouyang, M.G. Investigating the relationship between internal short circuit and thermal runaway of lithium-ion batteries under thermal abuse condition. *Energy Storage Mater.* **2021**, *34*, 563–573. [CrossRef]
7. Hong, J.C.; Wang, Z.P.; Yao, Y.T. Fault prognosis of battery system based on accurate voltage abnormity prognosis using long short-term memory neural networks. *Appl. Energy* **2019**, *251*, 14. [CrossRef]
8. Liu, J.; Tian, L.; Mou, Y.; Jia, W.; Zhang, L.; Liu, R. Electronic and mechanical property of high electron mobility semiconductor Bi_2O_2Se. *J. Alloys Compd.* **2018**, *764*, 674–678. [CrossRef]
9. Pang, Z.; Li, T. Mechanics and strain engineering of bulk and monolayer Bi_2O_2Se. *J. Mech. Phys. Solids* **2021**, *157*, 104626. [CrossRef]
10. Wang, Y.X.; Yan, Z.X.; Liu, W.; Zhou, G.L.; Gu, J.B. Ab initio study of the mechanical properties and thermal conductivity of Bi_2O_2X (X = Se, Te) under pressure. *Solid State Sci.* **2020**, *106*, 106299. [CrossRef]
11. Zhang, Z.; Chen, J.; Zhang, W.; Yu, Z.; Yu, C.; Lu, H. Systematically investigate mechanical and electrical properties of Bi_2O_2Se by Te atom substitution and compare it with homologue Bi_2O_2Te from first-principles calculations. *Mater. Today Commun.* **2020**, *24*, 101182. [CrossRef]
12. Piriz, S.; Fernandez-Werner, L.; Pardo, H.; Jasen, P.; Faccio, R.; Mombru, A.W. Mechanical properties and electronic structure of edge-doped graphene nanoribbons with F, O, and Cl atoms. *Phys. Chem. Chem. Phys.* **2017**, *19*, 21474–21480. [CrossRef] [PubMed]
13. Zhang, Z.; Gu, Y.; Wang, S.; Li, Q.; Li, M.; Zhang, Z. Enhanced dielectric and mechanical properties in chlorine-doped continuous CNT sheet reinforced sandwich polyvinylidene fluoride film. *Carbon* **2016**, *107*, 405–414. [CrossRef]
14. Park, H.; Woo, D.; Lee, J.M.; Park, S.J.; Lee, S.; Kim, H.J.; Yoon, E.; Lee, G.D. First principles investigation on energetics, structure, and mechanical properties of amorphous carbon films doped with B, N, and Cl. *Sci. Rep.* **2019**, *9*, 18961. [CrossRef]
15. Kresse, G.; Furthmüller, J. Efficient iterative schemes for ab initio total-energy calculations using a plane-wave basis set. *Phys. Rev. B* **1996**, *54*, 11169. [CrossRef] [PubMed]
16. Kresse, G.; Joubert, D. From ultrasoft pseudopotentials to the projector augmented-wave method. *Phys. Rev. B* **1999**, *59*, 1758. [CrossRef]
17. Qiao, L.; Zhang, S.; Xiao, H.Y.; Singh, D.J.; Zhang, K.H.L.; Liu, Z.J.; Zu, X.T.; Li, S. Orbital controlled band gap engineering of tetragonal $BiFeO_3$ for optoelectronic applications. *J. Mater. Chem. C* **2018**, *6*, 1239–1247. [CrossRef]
18. Heyd, J.; Scuseria, G.E.; Ernzerhof, M. Hybrid functionals based on a screened Coulomb potential. *J. Chem. Phys.* **2003**, *118*, 8207–8215. [CrossRef]
19. Monkhorst, H.J.; Pack, J.D. Special points for Brillouin-zone integrations. *Phys. Rev. B* **1976**, *13*, 5188–5192. [CrossRef]
20. Yao, H.; Ouyang, L.; Ching, W.-Y. Ab Initio Calculation of Elastic Constants of Ceramic Crystals. *J. Am. Ceram. Soc.* **2007**, *90*, 3194–3204. [CrossRef]
21. Wu, J.; Tan, C.; Tan, Z.; Liu, Y.; Yin, J.; Dang, W.; Wang, M.; Peng, H. Controlled Synthesis of High-Mobility Atomically Thin Bismuth Oxyselenide Crystals. *Nano Lett.* **2017**, *17*, 3021–3026. [CrossRef]
22. Chen, Q.; Zhang, P.; Qin, M.; Lou, Z.; Gong, L.; Xu, J.; Kong, J.; Yan, H.; Gao, F. Effect of La^{3+}, Ag^{+} and Bi^{3+} doping on thermoelectric properties of $SrTiO^3$: First-principles investigation. *Ceram. Int.* **2022**, *48*, 13803–13816. [CrossRef]
23. Boiler, I. Die Kristallstruktur von Bi_2O_2Se. *Monatsh. Chem.* **1973**, *104*, 916–919. [CrossRef]
24. Wu, J.; Yuan, H.; Meng, M.; Chen, C.; Sun, Y.; Chen, Z.; Dang, W.; Tan, C.; Liu, Y.; Yin, J.; et al. High electron mobility and quantum oscillations in non-encapsulated ultrathin semiconducting Bi_2O_2Se. *Nat. Commun.* **2017**, *12*, 530–534. [CrossRef] [PubMed]
25. Tan, X.; Lan, J.-L.; Ren, G.; Liu, Y.; Lin, Y.-H.; Nan, C.-W. Enhanced thermoelectric performance of n-type Bi_2O_2Se by Cl-doping at Se site. *J. Am. Ceram. Soc.* **2017**, *100*, 1494–1501. [CrossRef]
26. Hu, K.; Han, J.; Xu, B.; Lin, Y.H. Thermoelectric power factor of doped Bi_2O_2Se: A computational study. *Phys. Chem. Chem. Phys.* **2020**, *22*, 27096–27104. [CrossRef] [PubMed]
27. Li, J.Q.; Cheng, C.; Duan, M.Y. The electronic and optical properties of multi-layer Bi_2O_2X (X = S, Se, Te) by first-principles calculations. *Appl. Surf. Sci.* **2023**, *618*, 156541. [CrossRef]
28. Wang, Y.; Xu, B.; Yu, G.; Zhang, J.; Ma, S.; Yuan, S.; Sun, T.; Wang, Y. Electronic structure and thermoelectric properties of Bi_2O_2Se with GGA and TB-mBJ potentials. *Jpn. J. Appl. Phys.* **2019**, *58*, 015501. [CrossRef]
29. Yeh, J.W.; Chen, S.K.; Lin, S.J.; Gan, J.Y.; Chin, T.S.; Shun, T.T.; Tsau, C.H.; Chang, S.Y. Nanostructured high-entropy alloys with multiple principal elements: Novel alloy design concepts and outcomes. *Adv. Eng. Mater.* **2004**, *6*, 299–303. [CrossRef]
30. Li, M.; Wang, N.; Jiang, M.; Xiao, H.; Zhang, H.; Liu, Z.; Zu, X.; Qiao, L. Improved thermoelectric performance of bilayer Bi_2O_2Se by the band convergence approach. *J. Mater. Chem. C* **2019**, *7*, 11029–11039. [CrossRef]
31. Zhu, X.L.; Liu, P.F.; Xie, G.; Wang, B.T. First-principles study of thermal transport properties in the two- and three-dimensional forms of Bi_2O_2Se. *Phys. Chem. Chem. Phys.* **2019**, *21*, 10931–10938. [CrossRef] [PubMed]
32. Wang, F.; Di Valentin, C.; Pacchioni, G. Electronic and Structural Properties of WO^3: A Systematic Hybrid DFT Study. *J. Phys. Chem. C* **2011**, *115*, 8345–8353. [CrossRef]

33. Garza, A.J.; Scuseria, G.E. Predicting Band Gaps with Hybrid Density Functionals. *J. Phys. Chem. Lett.* **2016**, *7*, 4165–4170. [CrossRef] [PubMed]
34. He, J.; Franchini, C. Assessing the performance of self-consistent hybrid functional for band gap calculation in oxide semiconductors. *J. Phys. Condens. Matter* **2017**, *29*, 454004. [CrossRef] [PubMed]
35. Li, M.; Hu, J.; Gong, H.; Ren, Q.; Liao, Y.; Xiao, H.; Qiu, Q.; Feng, S.; Zu, X. First-principles study of point defects in U_3Si_2: Effects on the mechanical and electronic properties. *Phys. Chem. Chem. Phys.* **2022**, *24*, 4287–4297. [CrossRef]
36. Koc, H.; Ozisik, H.; Deligoz, E.; Mamedov, A.M.; Ozbay, E. Mechanical, electronic, and optical properties of $Bi(_2)S(_3)$ and $Bi(_2)Se(_3)$ compounds: First principle investigations. *J. Mol. Model.* **2014**, *20*, 2180. [CrossRef] [PubMed]
37. Chung, D.H.; Buessem, W.R. The Voigt-Reuss-Hill (VRH) Approximation and the Elastic Moduli of Polycrystalline ZnO, TiO_2 (Rutile), and α-Al_2O_3. *J. Appl. Phys.* **1968**, *39*, 2777–2782. [CrossRef]
38. Voigt, W. *Lehrbuch der Kristallphysik: Teubner-Leipzig*; Macmillan: New York, NY, USA, 1928; p. 739.
39. Reuss, A. Calculation of the flow limits of mixed crystals on the basis of the plasticity of monocrystals. *Z. Angew. Math. Mech.* **1929**, *9*, 49. [CrossRef]
40. Sagar, R.U.R.; Khan, U.; Galluzzi, M.; Aslam, S.; Nairan, A.; Anwar, T.; Ahmad, W.; Zhang, M.; Liang, T. Transfer-Free Growth of Bi_2O_2Se on Silicon Dioxide via Chemical Vapor Deposition. *ACS Appl. Electron. Mater.* **2020**, *2*, 2123–2131. [CrossRef]
41. Mahan, G.D. Figure of merit for thermoelectrics. *J. Appl. Phys.* **1989**, *65*, 1578–1583. [CrossRef]
42. Majumder, R.; Hossain, M.M. First-principles study of structural, electronic, elastic, thermodynamic and optical properties of topological superconductor LuPtBi. *Comput. Condens. Matter* **2019**, *21*, e00402. [CrossRef]
43. Nye, J.F.; Lindsay, R.B. Physical Properties of Crystals: Their Representation by Tensors and Matrices. *Phys. Today* **1957**, *10*, 26. [CrossRef]
44. Shi, X.; Chen, H.; Hao, F.; Liu, R.; Wang, T.; Qiu, P.; Burkhardt, U.; Grin, Y.; Chen, L. Room-temperature ductile inorganic semiconductor. *Nat. Mater.* **2018**, *17*, 421–426. [CrossRef] [PubMed]
45. Pugh, S.F. XCII. Relations between the elastic moduli and the plastic properties of polycrystalline pure metals. *Lond. Edinb. Dublin Philos. Mag. J. Sci.* **2009**, *45*, 823–843. [CrossRef]
46. Li, M.; Wang, N.; Zhang, S.; Hu, J.; Xiao, H.; Gong, H.; Liu, Z.; Qiao, L.; Zu, X. A review of the properties, synthesis and applications of lanthanum copper oxychalcogenides. *J. Phys. D Appl. Phys.* **2022**, *55*, 273002. [CrossRef]
47. MacIsaac, D.; Kanner, G.; Anderson, G. Basic physics of the incandescent lamp (lightbulb). *PhTea* **1999**, *37*, 520–525. [CrossRef]
48. Tvergaard, V.H.; Hutchinsonm, J.W. Microcracking in Ceramics Induced by Thermal Expansion or Elastic Anisotropy. *J. Am. Ceram. Soc.* **1988**, *71*, 157–166. [CrossRef]
49. Ravindran, P.; Fast, L.; Korzhavyi, P.A.; Johansson, B.; Wills, J.; Eriksson, O. Density functional theory for calculation of elastic properties of orthorhombic crystals: Application to $TiSi_2$. *J. Appl. Phys.* **1998**, *84*, 4891–4904. [CrossRef]
50. Gaillac, R.; Pullumbi, P.; Coudert, F.X. ELATE: An open-source online application for analysis and visualization of elastic tensors. *J. Phys. Condens. Matter* **2016**, *28*, 275201. [CrossRef] [PubMed]
51. Debye, P. Zur theorie der spezifischen wärmen. *Ann. Phys.* **1912**, *344*, 789–839.
52. Feng, J.; Xiao, B.; Wan, C.L.; Qu, Z.X.; Huang, Z.C.; Chen, J.C.; Zhou, R.; Pan, W. Electronic structure, mechanical properties and thermal conductivity of $Ln_2Zr_2O_7$ (Ln = La, Pr, Nd, Sm, Eu and Gd) pyrochlore. *Acta Mater.* **2014**, *72*, 1742–1760. [CrossRef]
53. Anderson, O.L. A simplified method for calculating the debye temperature from elastic constants. *J. Phys. Chem. Solids* **1963**, *24*, 909–917. [CrossRef]
54. Schreiber, E.; Anderson, O.L.; Soga, N.; Bell, J.F. Elastic constants and their measurement. *J. Appl. Mech.* **1975**, *42*, 747–748. [CrossRef]
55. Tian, J.; Zhao, Y.; Hou, H.; Wang, B. The Effect of Alloying Elements on the Structural Stability, Mechanical Properties, and Debye Temperature of $Al(_3)Li$: A First-Principles Study. *Materials* **2018**, *11*, 1471. [CrossRef] [PubMed]
56. Morelli, D.T.; Slack, G.A. *High Lattice Thermal Conductivity of Solids*; Springer: New York, NY, USA, 2006; pp. 37–68.
57. Li, Y.; Wang, J.; Wang, J. Approaching extremely low thermal conductivity by crystal structure engineering in $Mg_2Al_4Si_5O_{18}$. *J. Mater. Res.* **2015**, *30*, 3729–3739. [CrossRef]